

Coupling an Advanced Land Surface–Hydrology Model with the Penn State–NCAR MM5 Modeling System. Part I: Model Implementation and Sensitivity

FEI CHEN AND JIMY DUDHIA

National Center for Atmospheric Research, Boulder, Colorado

(Manuscript received 14 February 1999, in final form 25 July 2000)

ABSTRACT

This paper addresses and documents a number of issues related to the implementation of an advanced land surface–hydrology model in the Penn State–NCAR fifth-generation Mesoscale Model (MM5). The concept adopted here is that the land surface model should be able to provide not only reasonable diurnal variations of surface heat fluxes as surface boundary conditions for coupled models, but also correct seasonal evolutions of soil moisture in the context of a long-term data assimilation system. In a similar way to that in which the modified Oregon State University land surface model (LSM) has been used in the NCEP global and regional forecast models, it is implemented in MM5 to facilitate the initialization of soil moisture. Also, 1-km resolution vegetation and soil texture maps are introduced in the coupled MM5–LSM system to help identify vegetation/water/soil characteristics at fine scales and capture the feedback of these land surface forcings. A monthly varying climatological $0.15^\circ \times 0.15^\circ$ green vegetation fraction is utilized to represent the annual control of vegetation on the surface evaporation. Specification of various vegetation and soil parameters is discussed, and the available water capacity in the LSM is extended to account for subgrid-scale heterogeneity. The coupling of the LSM to MM5 is also sensitive to the treatment of the surface layer, especially the calculation of the roughness length for heat/moisture. Including the effect of the molecular sublayer can improve the simulation of surface heat flux. It is shown that the soil thermal and hydraulic conductivities and the surface energy balance are very sensitive to soil moisture changes. Hence, it is necessary to establish an appropriate soil moisture data assimilation system to improve the soil moisture initialization at fine scales.

1. Introduction

For more than a decade, it has been widely accepted that land surface processes and their modeling play an important role, not only in large-scale atmospheric models including general circulation models (GCMs) (e.g., Mintz 1981; Rowntree 1983, etc.), but also in regional and mesoscale atmospheric models (Rowntree and Bolton 1983; Ookouchi et al. 1984; Mahfouf et al. 1987; Avissar and Pielke 1989; Chen and Avissar 1994a,b, etc.). Mesoscale models that resolve wavelengths from 1 to 100 km (i.e., from meso- γ to meso- β scales) are often used for three applications: 1) regional climate simulations, 2) numerical weather prediction, and 3) air quality monitoring. Therefore, during the last few years, we have witnessed rapid progress in developing and testing land surface models in mesoscale atmospheric models (e.g., Bougeault et al. 1991; Giorgi et al. 1993; Bringfelt 1996; Smirnova et al. 1996; F. Chen et al. 1997; Pielke et al. 1997).

One key motivation behind this progress is that increasingly finer spatial and temporal resolutions and improved planetary boundary layer (PBL) parameterizations used in modern-era mesoscale numerical models permit us to realistically simulate the diurnal and vertical structure of the PBL. Due to their role of providing the surface boundary conditions to the atmosphere, the land surface processes are critical in influencing the PBL structure and associated clouds and precipitation processes. On the other hand, as mesoscale models continue to increase in spatial resolution, the density of the observation network is unable to capture the initial mesoscale structure at small scales. The majority of such mesoscale structures that are missed by the observation network are, in reality, a result of land surface forcing by topography, soil moisture, surface vegetation, and soil characteristics. Therefore, it is paramount that mesoscale models include an advanced and robust land surface model in order to properly initialize the state of the ground during a data assimilation period and to subsequently capture the mesoscale structures in the free atmosphere and PBL forced by the ground surface.

The fifth-generation Mesoscale Model (MM5), jointly developed by The Pennsylvania State University (Penn

Corresponding author address: Fei Chen, National Center for Atmospheric Research, P.O. Box 3000, Boulder, CO 80307.
E-mail: feichen@ncar.ucar.edu

State) and the National Center for Atmospheric Research (NCAR), is a mesoscale modeling system that includes advanced model physics. It is a community mesoscale model widely used for numerical weather prediction, air quality studies, and hydrological studies (Warner et al. 1991; Mass and Kuo 1998). Recently, the MM5 modeling and data assimilation system has been used for real-time weather prediction with grid increment as small as 1 km for the U.S. Army Test and Evaluation Command (Davis et al. 1999). Hence, correctly treating the land surface processes is becoming increasingly important for the model to be able to capture local mesoscale circulations induced by land surface forcing. The simple land surface model (LSM), conceptually a ground heat budget model, in the current official release of the MM5 model (Grell et al. 1994) is, however, not compatible with the complexity of other physics processes in this model. This simple LSM has the following major weaknesses: 1) the soil moisture field is defined as a function of land use and has only to seasonal values (summer and winter), but it does not change during the simulation and, hence, cannot reflect the impact of recent precipitation; 2) absence of snow cover prediction; 3) relatively coarse resolution land use; and 4) no vegetation evapotranspiration and runoff processes. Although there have been individual efforts to implement sophisticated LSMs in the MM5 and former MM4 system (Giorgi et al. 1993; Lakhtakia and Warner 1994, etc.), these codes are not generally available to the research community at large. In addition, the current MM5 coding structure is inadequate to accommodate the evolution of soil state variables such as soil moisture and snow depth. So, in the official release of the MM5, the simple model is the only LSM coupled to the MM5. Thus, the overall goals of this study are to 1) modify the structure of the MM5 modeling system so that it can easily host a series of LSMs developed by the research community, and 2) implement an advanced LSM to improve the simulation of surface heat fluxes, boundary layer, and precipitation processes.

Coupling a LSM in MM5, or generally speaking in mesoscale models, involves several complex issues. The first problem is to select an adequate but relatively simple LSM for real-time mesoscale weather and hydrology applications, because the computational time becomes a serious constraint for most such applications. The selection of the LSM is further complicated by the fact that most LSMs require a large number of parameters related to the vegetation and soil state. These parameters are difficult to specify at high resolution at continental scales. Another major problem is related to the initialization of soil moisture and temperature fields in the mesoscale models, because the soil moisture is a very important component in the land surface modeling system. Even in a "perfect LSM," inadequate initial soil moisture fields can introduce major biases in the partitioning of surface energy and have a long-lasting effect on the model behavior. Finally, it is necessary to vali-

date/test the coupled MM5–LSM system with available fields.

The objective of our study is to address and document the above issues in the context of coupling an LSM to the widely used community MM5 modeling system. Given the complexity of these issues, our research efforts will be presented in two parts. This first paper reviews problems and recent progress related to the selection of LSMs, the specification of land surface fields and various parameters, the initialization of soil moisture and temperature, and the coupling of the LSM to MM5. In the second paper (Chen and Dudhia 2001), we focus on our effort to validate the coupled MM5–LSM system against field observations.

2. Selection of the land surface model

Following the recognition of the importance of land surface processes in climate modeling systems, there have been significant efforts to attempt to more accurately represent the land–atmosphere interactions. As a result of this pursuit, a wide spectrum of LSMs have been developed in the last 20 years. One important work along this line is the introduction of a foliage layer (or "big leaf" model) in a soil model proposed by Deardorff (1978). In later LSM developments, this concept of explicitly treating the plant canopy has been adopted with variations. The explicit canopy treatment is modest in some models (e.g., Deardorff 1978; Pan and Mahrt 1987; Noilhan and Planton 1989) but rather complex in other models (e.g., Dickinson 1984; Sellers et al. 1986; Xue et al. 1991). The complex models employ a comprehensive treatment of biophysical and radiation interactions between the soil surface, vegetation, and the atmosphere. They, of course, have substantially more specified physical parameters than the more modest canopy models.

Another type of LSM (e.g., Entekhabi and Eagleson 1989; Wood et al. 1992; Schaake et al. 1996) is based on the understanding of the long-term hydrological cycle, and implicitly treats the effect of the vegetation canopy on evapotranspiration. Some of these hydrological models are designed and calibrated over large-scale river basins and incorporate the effects of subgrid-scale variability in precipitation and soil moisture. Some recent land surface modeling studies, particularly the Project for Intercomparison of Land-Surface Parameterization Schemes (PILPS) numerical experiments (Shao and Henderson-Sellers 1996; T. H. Chen et al. 1997; Wood et al. 1998), focused on the evaluation of different LSMs using long-term observations. These experiments showed that, given the same forcing conditions, the simulated surface heat fluxes, soil moisture, and runoff by different LSMs vary considerably. They also helped modelers to better understand the limitations of individual models. Partly motivated by these model intercomparison experiments, there are efforts to take the strengths of these LSMs originally designed for atmo-

spheric applications and apply them to surface hydrologic models or vice versa (Chen et al. 1996; Liang et al. 1999).

As pointed out by Chen et al. (1996), considering the significance of such a wide spectrum of land surface models, it is a big challenge for atmospheric modelers to select a land surface scheme that is appropriate to their needs. Furthermore, recent numerical experiments of intercomparing LSMs such as described in Chen et al. (1996) and in PILPS studies (T. H. Chen et al. 1997; Wood et al. 1998, etc.) revealed that sophisticated LSMs do not consistently outperform the relatively simple schemes. Partly, this is because it is difficult to accurately specify a potentially vast set of physical parameters, especially at the local scales required by some vegetation/soil/hydrology models.

In order to mitigate the aforementioned weaknesses of the overly simplified LSM in the MM5, a search was initiated for an appropriate LSM for weather prediction and hydrological applications. Based upon previous experience in dealing with land surface modeling in the National Centers for Environmental Prediction (NCEP) operational mesoscale Eta Model, the rationale adopted here is to select a LSM with relatively few parameters for real-time, year-round, and continental-domain application. The model, however, must still reflect the major effects of vegetation on the long-term evolution of surface evaporation and soil moisture.

Chen et al. (1996) extended the Oregon State University LSM (OSULSM), which was originally developed by Pan and Mahrt (1987), to include an explicit canopy resistance formulation used by Jacquemin and Noilhan (1990) and a surface runoff scheme of Schaake et al. (1996). They verified the performance of this LSM, alongside that of three other land surface parameterization schemes, from a very simple bucket model to a fairly complex simplified simple biosphere (SSiB) model, against 5 month First International Satellite Land Surface Climatology Project (ISLSCP) Field Experiment (FIFE) observations. It appears that this OSULSM is superior to the bucket model and performs similarly to the more sophisticated SSiB model. Tested against long-term observations, this LSM is able to reasonably reproduce the observed diurnal variation of sensible heat fluxes and surface skin temperature. Also, it is capable of capturing the diurnal and seasonal evolution in evaporation and soil moisture (Chen et al. 1996; T. H. Chen et al. 1997; Chen and Mitchell 1999).

This LSM was implemented in the NCEP operational Eta Model in February 1996, under the support of the National Atmospheric and Oceanic Administration's Global Energy and Water Cycle Experiment (GEWEX) Continental-Scale International Project program. Evaluated against field observations, the coupled Eta-OSULSM system indeed improves the short-range prediction of the surface heat fluxes, near-surface sensible variables, boundary layer, and precipitation (Betts et al. 1997; Chen et al. 1998; Yucel et al. 1998). Hence, con-

sidering its relative simplicity and adequate performance in the NCEP coupled Eta Model, this LSM is selected for implementation in the MM5 model. Another reason for selecting this LSM is that a similar LSM is used in the NCEP operational global and regional models, and this should facilitate the initialization of soil moisture in MM5 (a detailed discussion of the issue regarding the soil moisture initialization is given in section 5).

3. Brief description of the LSM

A brief description of the soil thermodynamics and soil hydrology in the OSULSM (see Fig. 1) is provided here. In particular, the focus will be on the model physics and parameters that have been changed from the LSM previously documented in Ek and Mahrt (1991) and Chen et al. (1996). This LSM is based on the coupling of the diurnally dependent Penman potential evaporation approach of Mahrt and Ek (1984), the multilayer soil model of Mahrt and Pan (1984), and the primitive canopy model of Pan and Mahrt (1987). It has been extended by Chen et al. (1996) to include the modestly complex canopy resistance approach of Noilhan and Planton (1989) and Jacquemin and Noilhan (1990). It has one canopy layer and the following prognostic variables: soil moisture and temperature in the soil layers, water stored on the canopy, and snow stored on the ground. For the soil model to capture the daily, weekly, and seasonal evolution of soil moisture and also to mitigate the possible truncation error in discretization, we use four soil layers, and the thickness of each layer from the ground surface to the bottom are 0.1, 0.3, 0.6, and 1.0 m, respectively. The total soil depth is 2 m, with the root zone in the upper 1 m of soil. Thus, the lower 1-m soil layer acts like a reservoir with a gravity drainage at the bottom. The depth of the vegetation roots can be specified as a function of vegetation type, if realistic rooting-depth data are available in the future.

a. Model thermodynamics

The surface skin temperature is determined following Mahrt and Ek (1984) by applying a single linearized surface energy balance equation representing the combined ground-vegetation surface. The ground heat flux is controlled by the usual diffusion equation for soil temperature (T):

$$C(\Theta) \frac{\partial T}{\partial t} = \frac{\partial}{\partial z} \left[K_t(\Theta) \frac{\partial T}{\partial z} \right]. \quad (1)$$

The volumetric heat capacity, C ($\text{J m}^{-3} \text{K}^{-1}$), and the thermal conductivity, K_t ($\text{W m}^{-1} \text{K}^{-1}$), are formulated as functions of volumetric soil water content, Θ [fraction of unit soil volume occupied by water; see Pan and Mahrt (1987)]:

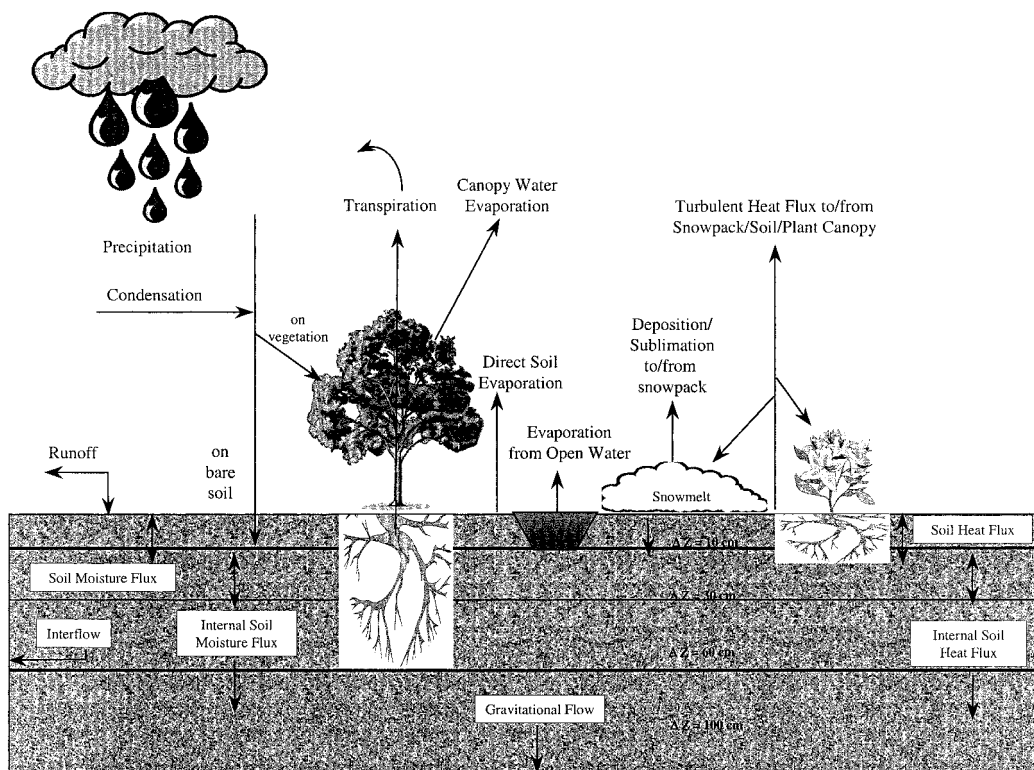


FIG. 1. A schematic representation of the OSULSM in the coupled MM5 model.

$$C = \Theta C_{\text{water}} + (1 - \Theta_s) C_{\text{soil}} + (\Theta_s - \Theta) C_{\text{air}}, \quad (2)$$

$$K_t(\Theta) = \begin{cases} 420 \exp[-(2.7 + P_f)], & P_f \leq 5.1 \\ 0.1744, & P_f > 5.1 < 0, \end{cases}$$

and

$$P_f = \log[\Psi_s(\Theta_s/\Theta)^b]. \quad (3)$$

The volumetric heat capacities are $C_{\text{water}} = 4.2 \times 10^6 \text{ J m}^{-3} \text{ K}^{-1}$, $C_{\text{soil}} = 1.26 \times 10^6 \text{ J m}^{-3} \text{ K}^{-1}$, and $C_{\text{air}} =$

$1004 \text{ J m}^{-3} \text{ K}^{-1}$. Here, Θ_s and Ψ_s are maximum soil moisture (porosity) and saturated soil potential (suction), respectively, and both depend on the soil texture (Cosby et al. 1984). The above function for computing the thermal conductivity (K_t), suggested by McCumber and Pielke (1981), has been used in numerous LSMs (e.g., Noilhan and Planton 1989; Viterbo and Beljaars 1995). The relationship between the volumetric soil moisture and thermal conductivity is illustrated in Fig. 2. Recently, Peters-Lidard et al. (1998) showed that, when compared to other formulations and the data collected in FIFE, this formulation tends to overestimate (underestimate) K_t during wet (dry) periods, and the surface heat fluxes are sensitive to the treatment of thermal conductivity. Hence, the maximum value of K_t is capped at $1.9 \text{ W m}^{-1} \text{ K}^{-1}$. We plan to test several thermal conductivity formulations in future studies, when relevant data are at our disposal.

The layer-integrated form of Eq. (1) for the i th soil layer is:

$$\Delta z_i C_i \frac{\partial T_i}{\partial t} = \left(K_t \frac{\partial T}{\partial z} \right)_{z_{i+1}} - \left(K_t \frac{\partial T}{\partial z} \right)_{z_i}. \quad (4)$$

The prediction of T_i is performed using the Crank–Nicholson scheme. The temperature at the lower boundary, assumed to be 3 m below the ground surface, is specified by the annual mean surface air temperature (see section 4 for detail). This also implies that the total

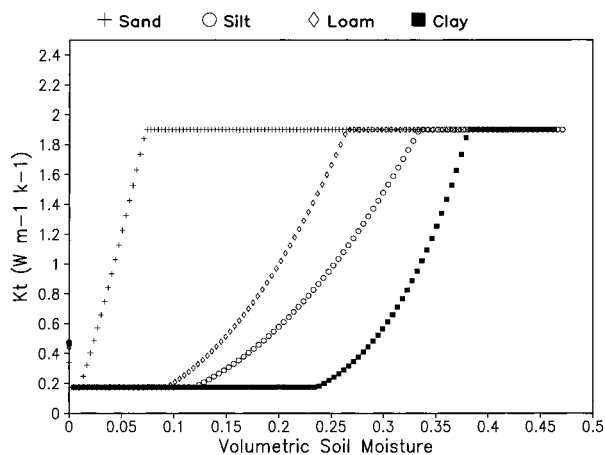


FIG. 2. Thermal conductivity as function of volumetric soil moisture for four soil types: sand, silt, loam, and clay.

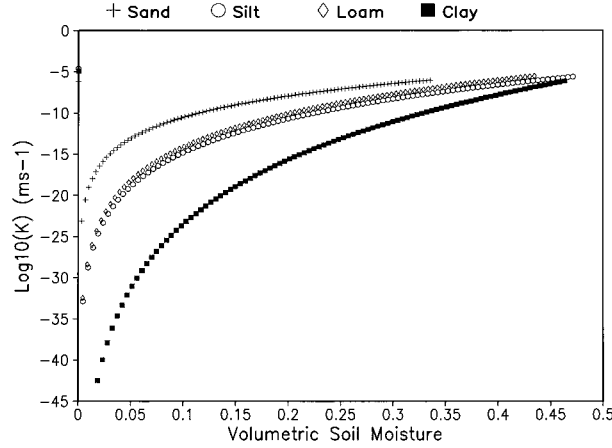


FIG. 3. Hydraulic conductivity as function of volumetric soil moisture for four soil types: sand, silt, loam, and clay.

soil column in the current LSM cannot exceed 3 m, although the number of layers is not limited.

b. Model hydrology

In the hydrology model, the prognostic equation for the volumetric soil moisture content (Θ) is

$$\frac{\partial \Theta}{\partial t} = \frac{\partial}{\partial z} \left(D \frac{\partial \Theta}{\partial z} \right) + \frac{\partial K}{\partial z} + F_{\Theta}, \quad (5)$$

where both the soil water diffusivity D and hydraulic conductivity K are functions of Θ , and F_{Θ} represents sources and sinks (i.e., precipitation, evaporation, and runoff) for soil water. This diffusive form of Richard's equation is derived from Darcy's law under the assumption of a rigid, isotropic, homogeneous, and one-dimensional vertical flow domain (Hanks and Ashcroft 1986), and thereby the soil water diffusivity D is given by $D = K(\Theta)(\partial \Psi / \partial \Theta)$ wherein Ψ is the soil water tension function. In Cosby et al. (1984), K and Ψ are computed by $K(\Theta) = K_s(\Theta/\Theta_s)^{2b+3}$ and $\Psi(\Theta) = \Psi_s/(\Theta/\Theta_s)^b$, where b is a curve-fitting parameter; K_s , Ψ_s , and b depend on soil type.

The hydraulic conductivity, K , as well as the diffusivity, D , are highly nonlinearly dependent on the soil moisture, as demonstrated in Fig. 3. It can change several orders of magnitude, even for a small variation in soil moisture, particularly when the soil is relatively dry. Cuenca et al. (1996) indicate that, for a bare-soil case, the diurnal partitioning of surface energy into latent heat and sensible heat is greatly affected by the soil water parameterization. Given such a sensitivity of hydraulic conductivity to soil moisture fluctuations and input soil properties, it is important to further investigate alternative parameterization schemes using better datasets to estimate the soil hydraulic properties in future studies.

Integrating Eq. (5) over four soil layers, as used in the MM5 model, and expanding F_{Θ} , we obtain

$$d_{z_1} \frac{\partial \Theta_1}{\partial t} = -D \left(\frac{\partial \Theta}{\partial z} \right)_{z_1} - K_{z_1} + P_d - R - E_{\text{dir}} - E_{t_1}, \quad (6)$$

$$d_{z_2} \frac{\partial \Theta_2}{\partial t} = D \left(\frac{\partial \Theta}{\partial z} \right)_{z_1} - D \left(\frac{\partial \Theta}{\partial z} \right)_{z_2} + K_{z_1} - K_{z_2} - E_{t_2}, \quad (7)$$

$$d_{z_3} \frac{\partial \Theta_3}{\partial t} = D \left(\frac{\partial \Theta}{\partial z} \right)_{z_2} - D \left(\frac{\partial \Theta}{\partial z} \right)_{z_3} + K_{z_2} - K_{z_3} - E_{t_3}, \quad (8)$$

and

$$d_{z_4} \frac{\partial \Theta_4}{\partial t} = D \left(\frac{\partial \Theta}{\partial z} \right)_{z_3} + K_{z_3} - K_{z_4}, \quad (9)$$

where d_{z_i} is the i th soil layer thickness, P_d the precipitation not intercepted by the canopy, and E_{ti} the canopy transpiration taken by the canopy root in the i th layer within the root zone layers (the root zone has three layers in the coupled MM5-LSM). At the bottom of the soil model, the hydraulic diffusivity is assumed to be zero, so that the soil water flux is due only to the "gravitational" percolation term K_{z_4} , also named subsurface runoff or drainage.

Following the recent trend to merge the traditional LSM with hydrological models to better represent the runoff mechanism, we adopt the surface runoff model in the Simple Water Balance (SWB) model to calculate the surface runoff R . The SWB model (Schaake et al. 1996) is a two-reservoir hydrological model that is typically calibrated for large river basins and that takes into account the spatial heterogeneity of rainfall, soil moisture, and runoff. The surface runoff, R , is defined as the excess of precipitation not infiltrated into the soil ($R = P_d - I_{\text{max}}$). The maximum infiltration, I_{max} , is formulated as

$$I_{\text{max}} = P_d \frac{D_x [1 - \exp(-kdt\delta_i)]}{P_d + D_x [1 - \exp(-kdt\delta_i)]},$$

$$D_x = \sum_{i=1}^4 \Delta Z_i (\Theta_s - \Theta_i), \quad \text{and} \quad kdt = kdt_{\text{ref}} \frac{K_s}{K_{\text{ref}}}, \quad (10)$$

where δ_i is the conversion of the current model time step δ_t (in terms of seconds) into daily values (i.e., $\delta_i = \delta_t/86400$); K_s is the saturated hydraulic conductivity, which depends on soil texture; and $kdt_{\text{ref}} = 3.0$ and $K_{\text{ref}} = 2 \times 10^{-6} \text{ m s}^{-1}$ are specified based on our PILPS 2(c) experiments (Wood et al. 1998). Further work needs to be done to calibrate these parameters over various basins with different precipitation climatologies.

The total evaporation, E , is the sum of 1) the direct evaporation from the top shallow soil layer, E_{dir} ; 2) evaporation of precipitation intercepted by the canopy, E_c ; and 3) transpiration via canopy and roots, E_t . That is, $E = E_{\text{dir}} + E_c + E_t$.

Based on a sensitivity test of Betts et al. (1997), we adopt here a simple linear method (Mahfouf and Noilhan

1991) for computing the direct evaporation from the ground surface:

$$E_{\text{dir}} = (1 - \sigma_f)\beta E_p \quad \text{and} \quad \beta = \frac{\Theta_1 - \Theta_w}{\Theta_{\text{ref}} - \Theta_w}, \quad (11)$$

where E_p is the potential evaporation, which is calculated by a Penman-based energy balance approach that includes a stability-dependent aerodynamic resistance (Mahrt and Ek 1984), Θ_{ref} and Θ_w are the field capacity and wilting point, and σ_f is the green vegetation fraction (cover), which is critical for the partitioning of total evaporation between bare soil direct evaporation and canopy transpiration.

The wet canopy evaporation is determined by

$$E_c = \sigma_f E_p \left(\frac{W_c}{S} \right)^n, \quad (12)$$

where W_c is the intercepted canopy water content, S is the maximum canopy capacity (chosen here to be 0.5 mm), and $n = 0.5$. This is similar to the formulations of Noilhan and Planton (1989) and Jacquemin and Noilhan (1990). The budget for intercepted canopy water is

$$\frac{\partial W_c}{\partial t} = \sigma_f P - D - E_c, \quad (13)$$

wherein P is the input total precipitation. If W_c exceeds S , the excess precipitation or drip, D , reaches the ground [note that $P_d = (1 - \sigma_f)P + D$ in Eq. (6)]. The canopy evapotranspiration is determined by

$$E_t = \sigma_f E_p B_c \left[1 - \left(\frac{W_c}{S} \right)^n \right], \quad (14)$$

where B_c is a function of canopy resistance and is formulated as

$$B_c = \frac{1 + \frac{\Delta}{R_r}}{1 + R_c C_h + \frac{\Delta}{R_r}}, \quad (15)$$

where C_h is the surface exchange coefficient for heat and moisture; Δ depends on the slope of the saturation specific humidity curve; R_r is a function of surface air temperature, surface pressure, and C_h ; and R_c is the canopy resistance. Details on C_h , R_r , and Δ are provided by Ek and Mahrt (1991). The canopy resistance, R_c , is calculated here following the formulation of Jacquemin and Noilhan (1990), where

$$R_c = \frac{R_{\text{cmin}}}{\text{LAI} F_1 F_2 F_3 F_4},$$

$$F_1 = \frac{R_{\text{cmin}}/R_{\text{cmax}} + f}{1 + f} \quad \text{where } f = 0.55 \frac{R_g}{R_{\text{gl}}} \frac{2}{\text{LAI}},$$

$$F_2 = \frac{1}{1 + h_s [q_s(T_a) - q_a]},$$

$$F_3 = 1 - 0.0016(T_{\text{ref}} - T_a)^2, \quad \text{and}$$

$$F_4 = \sum_{i=1}^3 \frac{(\Theta_i - \Theta_w) d_{z_i}}{(\Theta_{\text{ref}} - \Theta_w)(d_{z_1} + d_{z_2})}, \quad (16)$$

where F_1 , F_2 , F_3 , and F_4 are subject to 0 and 1 as lower and upper bounds and they represent the effects of solar radiation, vapor pressure deficit, air temperature, and soil moisture. Here, $q_s(T_a)$ is the saturated water vapor mixing ratio at the temperature T_a . The variable R_{cmin} is the minimum stomatal resistance, LAI is the leaf area index, and R_{cmax} is the cuticular resistance of the leaves and is set to 5000 s m⁻¹, as in Dickinson et al. (1993). The variable T_{ref} is 298 K according to Noilhan and Planton (1989). Note that the soil moisture stress function is only integrated in the root zone, which reaches the third soil layer in the current implementation. All other nonconstant parameters involved in the above equations will be discussed in the following section.

c. Snow and sea-ice model

Because this LSM is designed for application over a continental scale and should be able to deal with various surface characteristics, a simple snow and sea-ice model is included. The snow model has only one layer of snow cover and simulates the snow accumulation, sublimation, melting, and heat exchange at snow-atmosphere and snow-soil interfaces. The precipitation is categorized as snow when the temperature in the lowest atmospheric layer is below 0°C. The model estimates the heat flux between the soil and the snow by

$$G = K_{\text{snow}} \frac{T_s - T_{\text{soil}}}{D_{\text{snow}}}, \quad (17)$$

where T_s is the “skin” temperature, T_{soil} the temperature in the first soil layer, and D_{snow} the physical snow depth that is assumed to be 10 times the water-equivalent snow depth. Although the thermal diffusivity for snow, K_{snow} , depends on the porosity of snow, it is set to be 0.35 W m⁻¹ K⁻¹ in the present model.

Compared to the original OSULSM (Ek and Mahrt 1991), a new iterative procedure has been developed to represent the snow evaporation/sublimation and melting process. First, knowing the snow heat flux, G , enables one to calculate the potential evaporation E_p using the surface energy balance equation:

$$\begin{aligned}
& (1 - \alpha)S\downarrow + L\downarrow - \sigma T'^4 \\
& = G + \rho_0 C_p C_h |\mathbf{V}| (T' - T_a) \\
& \quad + \rho_0 L_v C_h |\mathbf{V}| [q_s(T') - q_a], \quad (18)
\end{aligned}$$

where ρ is the air density and C_p the air heat capacity. Here, $|\mathbf{V}|$ (wind speed), T_a , and q_a (air temperature and specific humidity) are evaluated at the lowest model level. The terms on the left-hand side are the downward short- and longwave surface radiation and the upward longwave radiation, while the terms on the right-hand side are the snow, sensible, and latent heat fluxes. The skin temperature T' is the temperature of the surface if the snow surface evaporates at the potential rate and is set to the snow surface temperature of the previous time step. The snow evaporates/sublimates at the following rate:

$$E = \begin{cases} E_p, & D_{\text{snow}} \geq E_p \delta_t \\ \frac{D_{\text{snow}}}{\delta_t}, & D_{\text{snow}} < E_p \delta_t. \end{cases}$$

Given E , the effective skin temperature, T_s , can be calculated by solving the surface energy balance equation:

$$\begin{aligned}
& (1 - \alpha)S\downarrow + L\downarrow - \sigma T_s^4 \\
& = K_s \frac{T_s - T_{\text{soil}}}{D_{\text{snow}}} + \rho_0 C_p C_h |\mathbf{V}| (T_s - T_a) + \text{LE}. \quad (19)
\end{aligned}$$

If the resultant T_s is below 0°C , snow will not melt. If $T_s > 0^\circ\text{C}$, evaporation/sublimation and melting will coexist, and the evaporation/sublimation will proceed at a potential rate at the snow surface temperature $T_c = 0^\circ\text{C}$, where $E = E_p = \rho_0 C_h |\mathbf{V}| [q_s(T_c) - q_a]$. Hence, the amount of snowmelt, h_m , which is allowed to drip into the top soil layer, is calculated as

$$\begin{aligned}
& (1 - \alpha)S\downarrow + L\downarrow - \sigma T_c^4 \\
& = K_s \frac{T_c - T_{\text{soil}}}{D_{\text{snow}}} + \rho_0 C_p C_h |\mathbf{V}| (T_c - T_a) + \text{LE} \\
& \quad + L_i h_m, \quad (20)
\end{aligned}$$

where L_i is the latent heat of fusion and T_c is the snow temperature that responds to both the evaporation/sublimation and melting of snow. If h_m is greater than the amount of snow left after the evaporation/sublimation, defined as h'_m , all the remaining snow (i.e., h'_m) will melt. In this case, a new surface skin temperature T_s will be determined by the surface energy balance:

$$\begin{aligned}
& (1 - \alpha)S\downarrow + L\downarrow - \sigma T_s^4 \\
& = K_s \frac{T_s - T_{\text{soil}}}{D_{\text{snow}}} + \rho_0 C_p C_h |\mathbf{V}| (T_s - T_a) + \text{LE} \\
& \quad + L_i h'_m. \quad (21)
\end{aligned}$$

Still, there are several weaknesses in this simple snow

model: 1) uniform snow cover over a given grid cell, 2) only one layer of snow, 3) constant thermal diffusivity for snow, and 4) no consideration of snow age and porosity. Recently, Koren et al. (1999) extended this LSM to include a physically based parameterization of frozen soil and a new snow accumulation/ablation scheme. This new scheme is able to simulate the total ice content of each soil layer. Tested against the data collected at the Rosemount site in Minnesota, the simulated soil temperature and unfrozen water content agreed with the observations reasonably well at different soil layers. Once this new snow and frozen soil physics is fully evaluated, it will be included in the coupled MM5.

As for the sea-ice model, because no data on ice thickness are routinely available, we attempt to get the simple aspects of the behavior right, rather than possibly overcomplicating the model when the initial data will never justify a sophisticated parameterization. Hence, a simple sea-ice model is implemented to account for the heat transfer among sea-ice layers and at sea-ice-atmosphere and sea-ice-sea interfaces. The sea-ice pack is divided into four equal layers with 0.75-m depth for each layer, and the total sea-ice pack is 3 m deep. An arbitrary 0.1-m snowpack is assumed to cover the sea-ice surface. The surface heat transfer and snow melting over the sea-ice surface is treated the same as in the snow model. The heat conduction equation [Eq. (4)] is also applied for the temperature in the sea-ice layers with three changes: 1) the heat capacity, C , for sea ice is $1.742 \times 10^6 \text{ J m}^{-3} \text{ K}^{-1}$; 2) the thermal conductivity, K_i , is $2.2 \text{ W m}^{-1} \text{ K}^{-1}$; and 3) the lower boundary condition for the sea-ice pack (i.e., the temperature at the sea surface below sea-ice pack) is assumed to be -2°C .

4. Land surface characteristic fields and parameter specification

In this LSM, there are two primary variables upon which other secondary parameters (such as minimal canopy resistance and soil hydraulic properties) are determined. These two variables are the vegetation type and the soil texture. For vegetation classification, we utilize the 1-km resolution U.S. Geological Survey's (USGS) SiB model vegetation categorization, which has 16 land cover classes (see Table 1). This land cover dataset is derived from the 1-km satellite Advanced Very High Resolution Radiometer (AVHRR) data obtained from April 1992 through March 1993. In fact, in addition to the SiB categories, this land cover dataset also provides several other land cover classifications (Loveland et al. 1995). Using North America as an example, in addition to the relatively simple 16-category (SiB land cover legend) classification there is a very detailed 205-category (seasonal land cover legend) classification. The USGS land cover data have been used in other regional coupled models (Pielke et al. 1997). Considering the difficulty in specifying physical parameters for a large

TABLE 1. Vegetation-related parameters in the LSM, which include roughness length (Z_0) in m, minimal stomatal resistance (R_{cmin}) in s m^{-1} . Here, R_{gl} is the visible solar flux for which F_1 [see Eq. (16)] is about to double its minimum value, and h_s is a parameter in F_2 .

Vegetation type	Albedo	Z_0 (m)	R_{cmin}	R_{gl}	h_s
1) Broadleaf-evergreen trees	0.11	2.653	150	30	41.69
2) Broadleaf-deciduous trees	0.12	0.826	100	30	54.53
3) Broadleaf and needleleaf trees	0.12	0.8	125	30	51.93
4) Needleleaf-evergreen trees	0.1	1.089	150	30	47.35
5) Needleleaf-deciduous trees (larch)	0.11	0.854	100	30	47.3
6) Broadleaf trees with groundcover	0.19	0.856	70	65	54.53
7) Groundcover only	0.19	0.075	40	100	36.35
8) Broadleaf shrubs with groundcover	0.25	0.238	300	100	42.0
9) Broadleaf shrubs with bare soil	0.25	0.065	400	100	42.0
10) Dwarf trees/shrubs with groundcover (tundra)	0.16	0.05	150	100	42
11) Bare soil	0.12	0.011			
12) Cultivations	0.19	0.075	40.0	100	36.35
13) Wetland	0.12	0.04	150	100	60
14) Dry coastal complex	0.19	0.075	400	100	200
15) Water	0.19	0.01			
16) Glacial	0.80	0.011	999	999	999

number of vegetation classifications at the microscale, we chose the 16-category SiB classification for the coupled MM5–LSM. However, we retain the capability of expanding it to include two or three additional categories to account for unique land cover types found in some limited areas. This 1-km resolution land use dataset provides not only a detailed spatial distribution of vegetation, but also a delineation between water bodies and land surface for MM5 high-resolution applications. When the MM5 horizontal grid increment is larger than 1 km, the dominant vegetation type in each grid box is selected to represent the “grid level” vegetation characteristics.

While the vegetation type is an annually invariant field, some vegetation characteristics may vary seasonally and can be specified either in lookup tables or in a satellite-derived dataset. Here, we adopt both techniques in the coupled MM5–LSM system. For instance, the green vegetation fraction, σ_f , defined as the grid-cell fraction for which midday downward solar insolation is intercepted by photosynthetically active green canopy, acts as a fundamental weighting coefficient in partitioning the total evaporation into the three components of evaporation. The sensitivity tests of Jacquemin and Noilhan (1990) and Betts et al. (1997) showed it to be an important first-order parameter. With improved technology, the remotely sensed data obtained from satellites provides excellent continuous estimates of the evolution of the vegetation state at global scales.

Sellers (1987) derived an important interrelationship among leaf area index (LAI), absorbed photosynthetically active radiation (APAR, which is closely related to the green vegetation cover), and satellite AVHRR/normalized difference vegetation index (NDVI). He found that under specified canopy properties, the APAR was linearly related to NDVI and curvilinearly related to LAI. It is, however, difficult to simultaneously derive LAI and σ_f from a single-product NDVI, unless one of them is prescribed. According to Gutman and Ignatov

(1998), it is more justified to prescribe LAI and derive σ_f . In addition, while σ_f and LAI are about equally important, the natural variability (a priori *uncertainty*) in σ_f seems substantially higher. Therefore, in the current coupled MM5–LSM, the LAI is prescribed, but σ_f is assigned by the monthly 5-yr climatology of green vegetation cover data with 0.15° resolution derived from AVHRR (Gutman and Ignatov 1998). The seasonal variation of this green vegetation fraction is shown in Fig. 4, wherein the green vegetation fraction in the agricultural areas located in the central and eastern United States dramatically changes from winter to the summer peak growing season. However, the LAI and σ_f should be allowed to change seasonally in the coupled model if future appropriate and consistent data become available.

Another critical vegetation parameter, which may be derived from satellite, is the surface albedo. Nevertheless, the spatial resolution of currently available albedo-climatology data are relatively coarse (e.g., the quarterly 1° albedo from the ISLSCP Initiative-I) compared to mesoscale model resolution of about 5–30 km. Hence, the albedo as well as the roughness length are specified according to the given dominant vegetation type, which has a higher resolution than the ISLSCP data, in the current model. Other vegetation-related physical parameters are compiled from various sources (e.g., Dorman and Sellers 1989; Dickinson et al. 1993; Mahfouf et al. 1995) and are listed in Table 1. Among these parameters, the minimum canopy resistance may be the most important one.

The soil texture is determined by using the 1-km resolution multilayer 16-category soil characteristics dataset developed by Miller and White (1998), which is based on the U.S. Department of Agriculture’s State Soil Geographic Database and provides information on the soil texture, bulk density, porosity, and available water capacity, etc. We use the soil texture class of the first surface soil layer in this dataset to apply to the soil

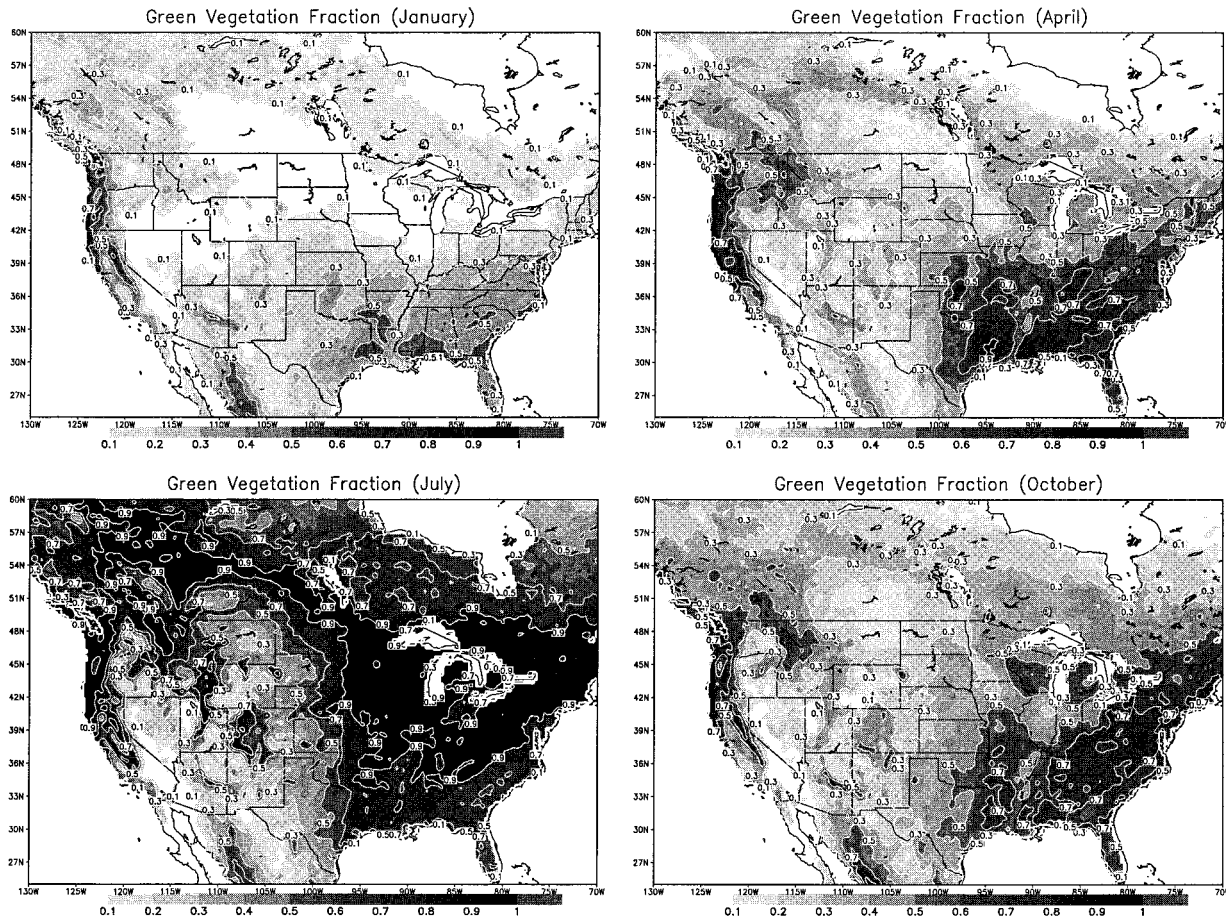


FIG. 4. Seasonal variation of NOAA/NESDIS 0.15° green vegetation fraction.

texture throughout the whole soil column for a given model grid cell. Four soil parameters, porosity (Θ_s), saturated metric potential (Ψ_s), saturated hydraulic conductivity (K_s), and slope of the retention curve (b), are

specified by the soil analysis of Cosby et al. (1984) (see Table 2).

The field capacity (Θ_{ref}) and wilting point (Θ_w) are not provided by Cosby et al. (1984) and need to be

TABLE 2. Soil-related parameters in the LSM. The hydraulic properties are volumetric water content at saturation (Θ_s), saturation soil suction (Ψ_s), hydraulic conductivity at saturation (K_s), field capacity (Θ_{ref}), and wilting point (Θ_w). Here, b is an exponent in the function that relates soil water potential and water content.

Soil type	Θ_s ($m^3 m^{-3}$)	Ψ_s (m)	K_s ($m s^{-1}$)	b	Θ_{ref} ($m^3 m^{-3}$)	Θ_w ($m^3 m^{-3}$)
1) Sand	0.339	0.069	1.07E-6	2.79	0.236	0.01
2) Loamy sand	0.421	0.036	1.41E-5	4.26	0.283	0.028
3) Sandy loam	0.434	0.141	5.23E-6	4.74	0.312	0.047
4) Silt loam	0.476	0.759	2.81E-6	5.33	0.36	0.084
5) Silt	0.476	0.759	2.81E-6	5.33	0.36	0.084
6) Loam	0.439	0.355	3.38E-6	5.25	0.329	0.066
7) Sandy clay loam	0.404	0.135	4.45E-6	6.66	0.314	0.067
8) Silty clay loam	0.464	0.617	2.04E-6	8.72	0.387	0.12
9) Clay loam	0.465	0.263	2.45E-6	8.17	0.382	0.103
10) Sandy clay	0.406	0.098	7.22E-6	10.73	0.338	0.1
11) Silty clay	0.468	0.324	1.34E-6	10.39	0.404	0.126
12) Clay	0.468	0.468	9.74E-7	11.55	0.412	0.138
13) Organic material	0.439	0.355	3.38E-6	5.25	0.329	0.06
14) Water						
15) Bedrock	0.25	7.59	9.74E-8	11.55	0.233	0.094
16) Other (land-ice)	0.421	0.036	1.34E-6	11.55	0.283	0.028

computed. The presumed water content at which internal drainage allegedly ceases, termed the field capacity, had, for a long time, been accepted almost universally in soil physics as an actual physical property for each soil type. However, there is no standard technique to measure or calculate it. In some literature, it is assigned to be 75% of the maximum soil moisture (porosity) (Noilhan and Planton 1989) or the soil moisture value when the hydraulic conductivity, K , equals 0.1 mm day^{-1} (Wetzel and Chang 1987). Yet, it is a very important parameter in the LSM formulations (11) and (16), which determine the evaporation rate, since it is assumed that there is no soil moisture stress when the soil moisture is above the field capacity. Here, we assume that a drainage flux of 0.5 mm day^{-1} through the bottom of the root zone is small enough to be disregarded and that the soil moisture at this drainage rate is equal to the field capacity. This criterion is given by Hillel (1980). The wilting point is defined as the critical soil moisture at (or below) which the evaporation process ceases; that is, it will be difficult to extract additional water that is closely tied to soil particles. As in Wetzel and Chang (1987), the wilting point is the soil moisture value when the soil water potential adjacent to the vegetation roots drops to -200 m with respect to the ground surface.

As indicated by Chen et al. (1996), the spatial distribution of soil moisture and, hence, evaporation is far from homogeneous in the natural world. For instance, even though the area-averaged soil moisture represented by a grid box of an atmospheric model is at the wilting point, the soil moisture in some subarea can be higher than the wilting point, and vice versa. Therefore, evaporation does occur over these subgrid areas and may be a significant contributor to the area-averaged latent heat flux during dry periods, as demonstrated by analysis of field observations (e.g., Stewart and Verma 1992). Chen et al. (1996) suggested that using a nonlinear soil moisture stress function can partly account for the soil moisture heterogeneity and can maintain a nonzero evaporation beyond the wilting point and reduce the evaporation when the area-averaged soil moisture is near the field capacity. This idea is adopted in the MM5-LSM, but we simply increase (decrease) the value of field capacity (wilting point) to save computational time. Thus, these two parameters are calculated for each soil type as

$$\Theta_{\text{ref}} = \Theta_s \left[\frac{1}{3} + \frac{2}{3} \left(\frac{5.79 \times 10^{-9}}{K_s} \right)^{1/(2b+3)} \right] \quad \text{and} \quad (22)$$

$$\Theta_w = 0.5 \Theta_s \left(\frac{200}{\Psi_s} \right)^{-1/b}. \quad (23)$$

To close the thermal diffusion equation [Eq. (4)], we need a lower boundary condition on temperature at 3 m below the ground surface. Because the observed soil temperature at this depth is not available, the annually averaged air temperature at 2 m is used as a substitute.

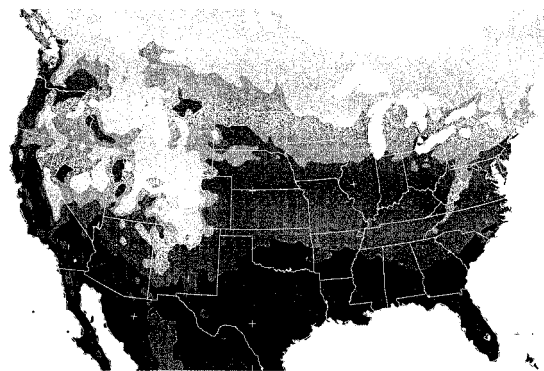


FIG. 5. Annual mean air temperature of 1987–88 adopted to the MM5 topography.

To our knowledge, the $1^\circ \times 1^\circ$ 2-m air temperature in the ISLSCP dataset is the only fine- (in a relative sense) resolution data available on the global scale. Although this 2-yr monthly 6-hourly 2-m air temperature is based on the European Centre for Medium-Range Weather Forecasts (ECMWF) model analysis and is strongly affected by the model physics, it looks very similar to the $5^\circ \times 5^\circ$ NCAR climatological 2-m temperature but shows finer structure due to its higher resolution. It, however, depends on the ECMWF model orography. Hence, this temperature is first adjusted to the 1000-mb level using the ECMWF annual analyzed surface pressure (also available from the ISLSCP dataset) according to the standard atmosphere lapse rate. It is then adjusted to the MM5 orography following the same procedure so it reflects the MM5 high-resolution topography, for instance over the Rocky Mountain areas as shown in Fig. 5.

5. Initialization of soil moisture

There is a rich literature demonstrating the importance of soil moisture, particularly its spatial heterogeneity, in mesoscale processes (e.g., Avissar and Pielke 1989; Chen and Avissar 1994a,b; Ziegler et al. 1995). Indeed, the soil moisture is a very important component of land surface modeling, and it would not make much sense to implement a sophisticated LSM in mesoscale models without a proper soil moisture initialization procedure. However, the initialization of soil moisture in coupled regional models is jeopardized by the fact that there are no routine soil moisture observations. Thus, until a soil moisture data assimilation system is developed for the MM5, the initialization of the LSM will largely depend on soil moisture fields obtained from analysis/forecasts from other models. Furthermore, as demonstrated by Koster and Milly (1997), different LSMs may have different soil moisture dynamic ranges

due to various approaches in treating evaporation and runoff.

In the current MM5–LSM model, the initial soil moisture can be obtained from two forecast/analysis systems, because a similar LSM is used in these systems and the soil moisture fields are compatible to the MM5–LSM with regard to its dynamic range. These two modeling systems are described as follows.

1) The NCEP regional operational Eta Model and its companion data assimilation system (EDAS) can be used. Because the Eta/EDAS system has relatively high resolution (running at 32 km since May 1998), its initial soil moisture can be useful for initializing the coupled MM5–LSM model over the North America region.

2) The NCEP–NCAR reanalysis system can be used for retrospective applications and the NCEP global data assimilation system (GDAS) can be used for real-time applications for regions outside of North America and for historical cases going back 40 yr. Nevertheless, some studies (e.g., Roads et al. 1997; Chen and Mitchell 1999) point out that the reanalysis tends to have very wet soil moisture due to a model positive precipitation bias, and thus a climatological soil moisture damping field is applied in the reanalysis system. In addition, the bias in the soil moisture fields in the reanalysis depends on season. Thus, when using NCEP–NCAR reanalysis or GDAS soil moisture fields to initialize the MM5 model, it may be necessary to adjust the soil moisture in the initialization procedure. The following formulations, based on several case studies conducted with the NCEP Eta Model while using the GDAS soil moisture as initial conditions, represent a possible choice for subjectively increasing (decreasing) the reanalysis–GDAS soil moisture from July to October (Jan–Jun).

When using the reanalysis–GDAS soil moisture to initialize the MM5 for January through June,

$$SM_{MM5} = \begin{cases} \min(0.7SM_g + 0.084, 0.35), & SM_g \geq 0.28 \\ SM_g, & \text{otherwise} \end{cases} \quad (24)$$

and for July through December,

$$SM_{MM5} = \begin{cases} 0.429SM_g + 0.16, & 0.21 < SM_g \leq 0.28 \\ 1.19SM_g, & SM_g \leq 0.21, \end{cases} \quad (25)$$

where SM_g is the soil moisture (in volumetric units) from the reanalysis–GDAS and SM_{MM5} is the initial soil moisture in the MM5 model. Such modest adjustments may, for instance, slightly decrease soil moisture in eastern and southern parts of the United States and increase soil moisture in western parts of the United States.

To demonstrate the sensitivity of the coupled MM5–LSM model to the initial soil moisture fields, the MM5 is set up to perform 48-h simulations (starting at 4 Jun

TABLE 3. Initial soil moisture fields in MM5–LSM four soil layers obtained from the interpolation of NCEP–NCAR reanalysis, at four locations.

Location	0.0–0.1-m soil layer	0.1–0.4-m soil layer	0.4–1.0-m soil layer	1–2-m soil layer
Dry point 1	0.16	0.16	0.15	0.14
Dry point 2	0.15	0.15	0.14	0.14
Semidry point	0.29	0.28	0.26	0.24
Wet point	0.39	0.38	0.36	0.34

1987). This period is chosen because of the existence of clear-sky conditions over most of the United States, which allows a better assessment of the land surface processes. The MM5 model is nested, and the horizontal grid increments are 90, 30, and 10 km. The initial soil moisture and temperature conditions in the MM5 are obtained from the NCEP–NCAR reanalysis, wherein, as mentioned, a similar LSM is used (Kalnay et al. 1996). For these sensitivity tests, two sets of simulations were conducted: 1) the soil moisture is changed (increased and decreased) by 10%, representing a relatively small change in soil moisture, with respect to the reanalysis values; and 2) the soil moisture is changed (increase and decrease) by 0.1 in terms of absolute volumetric values, representing a large change, with respect to the reanalysis values. In each of these simulations, the surface heat fluxes at four grid points are studied. These four points are located at 1) 35.01°N, 109.09°W, near the New Mexico and Arizona border for the 10% change experiment; 2) 35.01°N, 115.0°W, near Lake Havasu City, Arizona, for the 0.1 change experiment; 3) 34.11°N, 97.99°W, near Oklahoma City, Oklahoma; and 4) 34.11°N, 84.0°W, near Atlanta, Georgia, for both experiments. The first two points represent dry climatology, and the third and the fourth points represent semidry and wet climatology, respectively. Note that the reanalysis volumetric soil moisture fields are for two soil layers, 0–10 and 10–200 cm, and are interpolated to the four soil layers in the MM5–LSM. The initial soil moisture, interpolated from the reanalysis, for the four soil layers at the above four points, are listed in Table 3.

The responses of the coupled model surface heat flux to the initial soil moisture changes are shown in Figs. 6 and 7 for the two dry points and the semidry point. The largest impact of soil moisture on the surface heat fluxes is found for dry soils. At the initial soil moisture value of 0.16, a small change of 10% in initial soil moisture can result in a 30 W m⁻² variation in surface heat fluxes. The influence of initial soil moisture on the surface heat fluxes seems to be carried over into the 24–48-h simulation period. The change of 0.1 in the initial soil moisture in terms of its volumetric value can cause a change of about 200 W m⁻². Even for a relatively moist soil (see Fig. 7), the uncertainty in initial soil moisture appears to have similar effect on the surface heat flux in the coupled model for a period of up

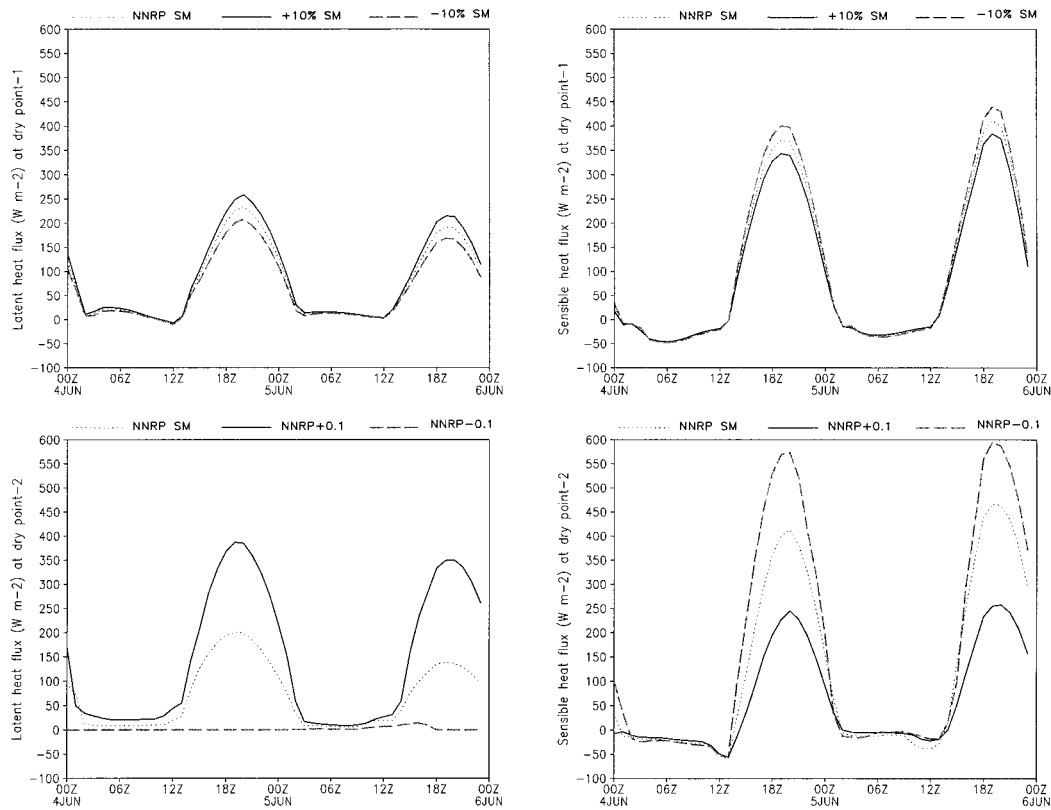


FIG. 6. Sensitivity of surface heat fluxes to the initial soil moisture for two dry points.

to, at least, 48 h. For the wet soil case, because the initial soil moisture (0.36–39) is higher than the field capacity (0.312 for the loamy sand at the wet point), the surface heat flux is only slightly changed with both the 10% and 0.1 variations in initial soil moisture (not shown here), as expected. Thus, this perturbation in initial soil moisture seems to primarily affect the surface energy balance in dry and semidry areas.

Note that obtaining the initial soil moisture with an accuracy of 10% at continental scales is beyond our current capability. First, there are no routine observations of high-resolution soil moisture at large scales. Second, because the precipitation and surface radiation are not restricted (or assimilated) in the traditional four-dimensional data assimilation systems, the soil moisture fields suffer from model errors in radiation and precipitation. For instance, the ECMWF operational global model had problems related to large drifts in soil moisture, which, in turn, affected the precipitation forecasts (Viterbo and Courtier 1995). Thus, several major numerical prediction centers have suggested different approaches in order to mitigate these problems (e.g., Boutier et al. 1993; Mitchell 1994; Smith et al. 1994). Among these methods is the idea of using observed precipitation and surface radiation to drive an LSM in offline mode to simulate long-term evolution of soil moisture. This is appealing for regional model applications, wherever high-resolution (spatial and temporal)

precipitation observations are available. The rationale behind this idea is that, according to recent studies (Chen and Mitchell 1999; Calvet et al. 1998), the evolution of soil moisture in the surface layer and in the deep root zone can be reasonably well captured by land surface models, given accurate atmospheric and surface forcing conditions.

The future development of a soil moisture data assimilation system for the coupled MM5–LSM model will certainly depend on the region of intended application. If high-resolution precipitation and surface radiation are available, an offline soil moisture simulation system may be a good solution. In other regions, the long-term solution is to explore the possibility of utilizing variational analysis to assimilate the surface soil moisture with information obtained from remote sensing.

6. Surface layer parameterization and PBL scheme

The LSM is coupled to the MM5 model through the lowest atmospheric level, which is also referred to as the surface layer. A surface layer parameterization should provide the surface (bulk) exchange coefficients for momentum, heat, and water vapor used to determine the flux of these quantities between the land surface and the atmosphere. The surface layer parameterization ba-

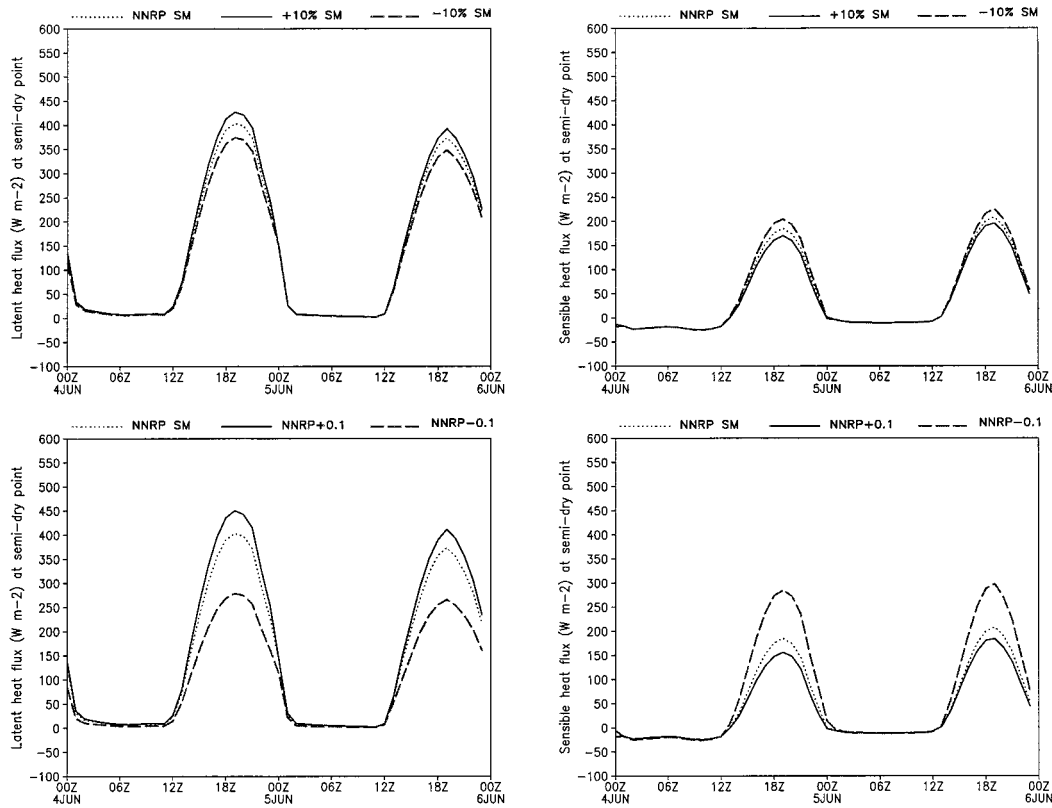


FIG. 7. Sensitivity of surface heat fluxes to the initial soil moisture for a semidry point.

ses its surface flux calculations on similarity theory, using a stability-dependent function (ψ_h) and roughness length to determine the surface exchange coefficient for heat and moisture. This exchange coefficient is passed to the LSM from the PBL scheme, together with surface radiative forcing terms and precipitation rate. The LSM routine returns to the PBL scheme the surface heat and moisture fluxes for calculation of the boundary layer flux convergence, which contributes to atmospheric temperature and moisture tendencies. The LSM essentially replaces the current MM5 ground temperature prediction calculation that is based on the energy budget at the ground.

Currently, in MM5, the surface exchange coefficient for heat and moisture is formulated as

$$C_h = \frac{k^2 V_a}{\left[\ln\left(\frac{z_a}{z_{0m}}\right) - \psi_m \right] \left[\ln\left(\frac{z_a}{z_{0t}}\right) - \psi_h \right]}, \quad (26)$$

where ψ_m and ψ_h are expressed as in Eq. (5) of Oncley and Dudhia (1995). However, MM5 now uses a lookup table to fit the function instead of a polynomial fit for unstable conditions. The variable z_a is the height above ground of the lowest computation level in the model (typically 35 m), k (0.4) is the von Kármán constant, and V_a is the wind speed at the lowest layer. The quantities z_{0m} and z_{0t} are the roughness lengths for momen-

tum and heat, respectively. Derived from Carlson and Boland (1978), z_{0t} is defined as

$$z_{0t} = \frac{1}{\left(\frac{ku_*}{K_a} + \frac{1}{z_l} \right)}, \quad (27)$$

where K_a is the molecular diffusivity ($2.4 \times 10^{-5} \text{ m}^2 \text{ s}^{-1}$) and u_* is the friction velocity. Note that the formulation includes the molecular sublayer through the parameter z_l ($=0.01 \text{ m}$), and this was previously only applied to moisture in MM5. The LSM's use of a skin temperature, which is defined at the surface not at z_{0m} , as opposed to the previously used slab-layer ground temperature, makes this formulation more consistent with Monin–Obukhov similarity theory. The effect of the molecular sublayer is to act as a resistance to fluxes, and it is equivalent in this sense to the use of smaller thermal roughness lengths as proposed by several authors. For example, F. Chen et al. (1997) tested two approaches to specify the thermal roughness length: 1) assume the roughness length for heat is a fixed ratio of the roughness length for momentum, and 2) relate this ratio to the roughness Reynolds number as proposed by Zilitinkevich (1995). Their 1D column model sensitivity tests suggested that the Zilitinkevich approach can improve the surface heat flux and skin temperature simulations. A long-term test with the NCEP mesoscale Eta

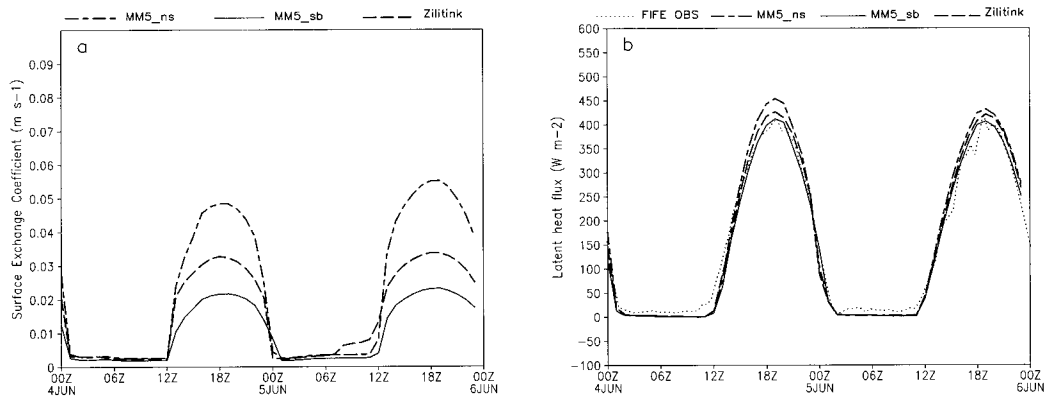


FIG. 8. (a) Comparison of surface exchange coefficients calculated using three functions: 1) MM5_{ns}, without using the sublayer parameterization; 2) MM5_{sb}, with sublayer parameterization as in Eq. (27); and 3) the Zilitinkevich scheme. (b) Comparison of latent heat fluxes of these three schemes and the FIFE observations.

Model indicated that this approach can also reduce forecast precipitation bias.

Figure 8 shows a comparison of surface exchange coefficients calculated by three methods. Without a sublayer parameterization [i.e., $z_{om} = z_{ot}$ in Eq. (26)] the surface exchange coefficients are overestimated and can double the values compared to using a sublayer parameterization [Eq. (27)]. Verified against the area-averaged latent heat flux obtained from the FIFE observations (Betts and Ball 1998), the simulation without the sublayer parameterization tends to overestimate the surface heat fluxes. Although the surface exchange coefficients using the Zilitinkevich scheme with parameter $C = 0.1$ are higher than that obtained using Eq. (27), the latent heat fluxes calculated by both methods are very close and the MM5 sublayer scheme produces slightly better results during the day.

The land surface model interacts with MM5 through its boundary layer scheme. Currently, the LSM has been coupled with the nonlocal PBL scheme based on Troen and Mahrt (1986) and that has been implemented in the NCEP Medium-Range Forecast (MRF) model by Hong and Pan (1996). Compared with other nonlocal or high-order closure schemes, this PBL scheme has a similar performance but is more efficient.

7. Summary

This paper has addressed a number of issues related to the implementation of an advanced land surface–hydrology model in the Penn State–NCAR MM5 modeling system. The overall philosophy is to select a relatively simple and sound land surface model, so that it can be efficiently executed for real-time atmospheric and hydrologic applications at different scales. One concept adopted here is that the LSM should be able to provide not only reasonable diurnal variations of surface heat fluxes (which is, of course, the primary function of an LSM), but also correct seasonal evolutions of soil moisture in the context of a long-term data assimilation sys-

tem. This, in turn, will ensure the accurate partitioning of available surface energy into latent and sensible heating. The modified OSULSM (Chen et al. 1996) has been tested against field observations obtained for various climate and vegetation/soil conditions. This LSM performs adequately in the NCEP mesoscale forecast Eta Model, and a similar LSM is also used in the NCEP global data assimilation system and NCEP–NCAR reanalysis system. Considering the issue of the compatibility of the soil moisture dynamic range, which represents a difficulty in utilizing one LSM's soil moisture to initialize another LSM that may have a different soil moisture climatology, employing this LSM should facilitate the soil moisture initialization for the MM5 model. This is one of the major reasons that this LSM was chosen for implementation in the MM5 model.

To meet the increasing demand for employing high-resolution mesoscale models (e.g., 1-km horizontal spacing), several high-resolution fields characterizing the land surface conditions are utilized in the coupled MM5–LSM model. For instance, the 1-km resolution land use and soil texture maps will help identify vegetation/water/soil characteristics at finescales, and capture the dynamics of the associated land surface forcing. This is important for inducing mesoscale atmospheric circulations and modifying the development of the PBL and associated cloud and precipitation processes, as demonstrated by many studies (Avisar and Pielke 1989; Chen and Avisar 1994a,b, etc.) Note that these land surface forcings seem to not only influence the local circulations but also to modify large-scale precipitation processes, even in some situations that are dominated by strong synoptic forcing during warm seasons (Beljaars et al. 1996; Paegle et al. 1996). A monthly varying climatology $0.15^\circ \times 0.15^\circ$ green vegetation fraction is also introduced in the MM5–LSM coupled model to represent the annual control of vegetation on the partitioning of total vegetation among bare soil direct evaporation in the surface layer and canopy uptake of water in deep root zones. Given the important role of the land

use and soil texture in determining secondary parameters in the LSM, and the green vegetation fraction to the seasonal evolution of evaporation and soil moisture, it is necessary to evaluate these surface fields in order to further improve their characterizations in coupled models.

In this coupled MM5–LSM system, the secondary vegetation and soil properties such as albedo, minimum stomatal resistance, and soil thermal/hydraulic conductivity are determined by the spatial distribution of vegetation and soil types. Some of these parameters are simply compiled from the literature, and some of them are calculated from widely used formulations. The available water capacity, which is the difference between the field capacity and wilting point, is expanded to take into account the surface heterogeneity in soil moisture fields. In the future, increasingly improved remote sensing techniques can help the real-time specification of the seasonal evolution of some vegetation and soil parameters such as albedo, LAI, roughness length, etc., in the coupled model.

The soil thermal and hydraulic conductivities, being critical for heat and soil water transfer within the soil layers, are very sensitive to soil moisture changes. This will certainly affect the soil water movement and runoff processes. Furthermore, the partitioning of surface radiation forcing into latent and sensible heat fluxes are also significantly influenced by the initial soil moisture fields, especially in arid and semiarid climatic regions. Thus, although the current coupled MM5–LSM can utilize the soil moisture analyzed/forecasted by the NCEP global and regional operational assimilation/forecast systems, it is necessary to establish an appropriate soil moisture data assimilation system to improve the soil moisture initialization at finescales. Such a system can be based on an offline LSM and use the observed precipitation and surface radiation as forcing conditions.

The issue of coupling the LSM to the surface layer (i.e., the lowest model level in the MM5) cannot be overlooked. It involves the formulations for calculating the surface exchange coefficients and, in particular, the treatment of the roughness length for heat/moisture. The formulation, which includes the molecular sublayer, can reduce the surface exchange coefficient for the unstable regime and hence mitigate the overestimation of surface heat fluxes. Although the surface exchange coefficients calculated from the MM5 molecular sublayer formulation are somewhat lower than those from the Zilitinkevich scheme tested by F. Chen et al. (1997), the surface heat fluxes obtained from these two formulations are very similar and agree with the FIFE observations.

This paper documents a significant extension to the widely used community MM5 modeling system, which will extend its applicability to long-term simulations by allowing soil moisture variations, as well as improve short-range forecasts by allowing for initial land surface inhomogeneities that were previously neglected. By releasing this LSM to a broad user community, it is ex-

pected that its usage in scientific studies will greatly increase, and more expertise will be available for verifying it in detail, as well as for suggesting and making future improvements to the LSM and its coupling to MM5. Furthermore, since the MM5 system now has in place the linkages for one LSM, it is expected that developing options for other LSMs will be easier.

Acknowledgments. This research was funded by the U.S. Army Test and Evaluation Command through an Interagency Agreement with the National Science Foundation, the special funds from the National Science Foundation that have been designated for the U.S. Weather Research Program at NCAR, and DOE/ARM Grant DE-AI02-97ER62359. We express our appreciation to Dr. Thomas Warner for his support and suggestions. Many have helped to make the OSULSM part of MM5's version 3 release in the summer of 1999. Yong-Run Guo provided a means of including vegetation, soil, and vegetation fraction among the standard modeling system datasets. Kevin Manning has helped with the extraction of soil moisture and temperature and other information from the NNRP and EDAS archived data, and with manipulating the Level II rainfall data. David Gill has adapted programs to interpolate new surface datasets onto the model grid. Wei Wang has facilitated use of the LSM in the standard version 3 release available to MM5 users. Lynn Berry has prepared some of the figures presented in this paper.

REFERENCES

- Avisar, R., and R. Pielke, 1989: A parameterization of heterogeneous land surfaces for atmospheric numerical models and its impact on regional meteorology. *Mon. Wea. Rev.*, **117**, 2113–2136.
- Beljaars, A. C. M., P. Viterbo, M. Miller, and A. Betts, 1996: The anomalous rainfall over the United States during July 1993: Sensitivity to land surface parameterization and soil moisture anomalies. *Mon. Wea. Rev.*, **124**, 362–383.
- Betts, A. K., and J. H. Ball, 1998: FIFE surface climate and site-average dataset 1987–89. *J. Atmos. Sci.*, **55**, 1091–1108.
- , F. Chen, K. Mitchell, and Z. Janjic, 1997: Assessment of land surface and boundary layer models in two operational versions of the NCEP Eta Model using FIFE data. *Mon. Wea. Rev.*, **125**, 2896–2915.
- Bougeault, P., J. Noilhan, P. Lacarrere, and P. Mascart, 1991: An experiment with an advanced surface parameterization in a mesobeta-scale model. Part I: Implementation. *Mon. Wea. Rev.*, **119**, 2358–2373.
- Bouttier, F., J. F. Mahfouf, and J. Noilhan, 1993: Sequential assimilation of soil moisture from atmospheric low-level parameters. Part I: Sensitivity and calibration studies. *J. Appl. Meteor.*, **32**, 1335–1351.
- Bringfelt, B., 1996: Tests of a new land surface treatment in HIRLAM. HIRLAM Tech. Rep. 23, Swedish Meteorological and Hydrological Institute, Norrköping, Sweden, 72 pp.
- Calvet, J. C., J. Noilhan, and P. Bessemoulin, 1998: Retrieving the root-zone soil moisture from surface soil moisture or temperature estimates: A feasibility study based in field measurements. *J. Appl. Meteor.*, **37**, 371–386.
- Carlson, T. N., and F. E. Boland, 1978: Analysis of urban–rural canopy using a surface heat flux/temperature model. *J. Appl. Meteor.*, **17**, 998–1013.

- Chen, F., and R. Avissar, 1994a: The impact of land-surface wetness on mesoscale heat fluxes. *J. Appl. Meteor.*, **33**, 1324–1340.
- , and —, 1994b: Impact of land-surface moisture variability on local shallow convective cumulus and precipitation in large-scale models. *J. Appl. Meteor.*, **33**, 1382–1401.
- , and K. Mitchell, 1999: Using GEWEX/ISLSCP forcing data to simulate global soil moisture fields and hydrological cycle for 1987–1988. *J. Meteor. Soc. Japan*, **77**, 1–16.
- , and J. Dudhia, 2001: Coupling an advanced land surface–hydrology model with the Penn State–NCAR MM5 Modeling system. Part II: Preliminary model validation. *Mon. Wea. Rev.*, **129**, 587–604.
- , and Coauthors, 1996: Modeling of land-surface evaporation by four schemes and comparison with FIFE observations. *J. Geophys. Res.*, **101**, 7251–7268.
- , J. Dudhia, Z. Janjic, and M. Baldwin, 1997: Coupling a land-surface model to the NCEP mesoscale Eta model. Preprints, *13th Conf. on Hydrology*, Long Beach, CA, Amer. Meteor. Soc., 99–100.
- , —, —, and —, 1998: Impact of land-surface processes on the NCEP Eta model quantitative precipitation forecast. Preprints, *Special Symp. on Hydrology*, Phoenix, AZ, 281–282.
- Chen, T. H., and Coauthors, 1997: Cabauw experimental results from the Project for Intercomparison of Land-surface Parameterization Schemes. *J. Climate*, **10**, 1194–1215.
- Cosby, B. J., G. M. Hornberger, R. B. Clapp, and T. R. Ginn, 1984: A statistical exploration of the relationships of soil moisture characteristics to the physical properties of soils. *Water Resour. Res.*, **20**, 682–690.
- Cuenca, R. H., M. Ek, and L. Mahrt, 1996: Impact of soil water property parameterization on atmospheric boundary-layer simulation. *J. Geophys. Res.*, **101**, 7269–7277.
- Davis, C., T. Warner, E. Astling, and J. Bowers, 1999: Development and application of an operational, relocatable, meso-gamma-scale weather analysis and forecasting system. *Tellus*, **51A**, 710–727.
- Deardorff, J. W., 1978: Efficient prediction of ground surface temperature and moisture, with inclusion of a layer of vegetation. *J. Geophys. Res.*, **83**, 1889–1903.
- Dickinson, R. E., 1984: Modeling evapotranspiration for three-dimensional global climate models. *Climate Processes and Climate Sensitivity: Maurice Ewing Volume 5, Geophys. Monogr.*, No. 29, Amer. Geophys. Union, 58–72.
- , A. Henderson-Sellers, and P. J. Kennedy, 1993: Biosphere–Atmosphere Transfer Scheme (BATS) Version 1e as coupled to the NCAR Community Climate Model. NCAR Tech. Note NCAR/TN-387 + STR, 72 pp.
- Dorman, J. L., and P. J. Sellers, 1989: A global climatology of albedo, roughness length and stomatal resistance for atmospheric general circulation models as represented by the Simple Biosphere Model (SiB). *J. Appl. Meteor.*, **28**, 833–855.
- Ek, M., and L. Mahrt, 1991: OSU 1-D PBL model user's guide. Version 1.04, 120 pp. [Available from Department of Atmospheric Sciences, Oregon State University, Corvallis, OR 97331-2209.]
- Entekhabi, D., and P. S. Eagleson, 1989: Land surface hydrology parameterization for atmospheric general circulation models including subgrid scale variability. *J. Climate*, **2**, 816–831.
- Giorgi, F., M. R. Marinucci, and G. Bates, 1993: Development of a second-generation regional climate model (RegCM2). Part II: Convective processes and assimilation of lateral boundary conditions. *Mon. Wea. Rev.*, **121**, 2814–2832.
- Grell, G., J. Dudhia, and D. Stauffer, 1994: A description of the fifth-generation Penn State/NCAR Mesoscale Model (MM5). NCAR Tech. Note NCAR/TN-398 + STR, 117 pp.
- Gutman, G., and A. Ignatov, 1998: The derivation of green vegetation fraction from NOAA/AVHRR data for use in numerical weather prediction models. *Int. J. Remote Sens.*, **19**, 1533–1543.
- Hanks, R. J., and G. L. Ashcroft, 1986: *Applied Soil Physics*. Springer-Verlag, 159 pp.
- Hillel, D., 1980: *Applications of Soil Physics*. Academic Press, 385 pp.
- Hong, S.-Y., and H.-L. Pan, 1996: Nonlocal boundary layer vertical diffusion in a medium-range forecast model. *Mon. Wea. Rev.*, **124**, 2322–2339.
- Jacquemin, B., and J. Noilhan, 1990: Sensitivity study and validation of a land surface parameterization using the HAPEX-MOBILHY data set. *Bound.-Layer Meteor.*, **52**, 93–134.
- Kalnay, E., and Coauthors, 1996: The NCEP/NCAR 40-Year Reanalysis Project. *Bull. Amer. Meteor. Soc.*, **77**, 437–471.
- Koren, V., J. Schaake, K. Mitchell, Q.-Y. Duan, and F. Chen, 1999: A parameterization of snowpack and frozen ground intended for NCEP weather and climate models. *J. Geophys. Res.*, **104**, 19 569–19 585.
- Koster, R., and C. P. Milly, 1997: The interplay between transpiration and runoff formulations in land surface schemes used with atmospheric models. *J. Climate*, **10**, 1578–1591.
- Lakhtakia, M. N., and T. T. Warner, 1994: A comparison of simple and complex treatments of surface hydrology and thermodynamics suitable for mesoscale atmospheric models. *Mon. Wea. Rev.*, **122**, 880–896.
- Liang, X., E. F. Wood, and D. P. Lettenmaier, 1999: Modeling ground heat flux in land surface parameterization schemes. *J. Geophys. Res.*, **104**, 9581–9602.
- Loveland, T. R., J. W. Merchant, J. F. Brown, D. O. Ohlen, B. C. Reed, P. Olson, and J. Hutchinson, 1995: Seasonal land-cover regions of the United States. *Ann. Assoc. Amer. Geogr.*, **85**, 339–355.
- Mahfouf, J. F., and J. Noilhan, 1991: Comparative study of various formulation from bare soil using in situ data. *J. Appl. Meteor.*, **30**, 1354–1365.
- , E. Richard, and P. Mascart, 1987: The influence of soil and vegetation on the development of mesoscale circulations. *J. Climate Appl. Meteor.*, **26**, 1483–1495.
- , A. O. Manzi, J. Noilhan, H. Giordani, and M. Deque, 1995: The land surface scheme ISBA within the Meteo-France climate model ARPEGE. Part I: Implementation and preliminary results. *J. Climate*, **8**, 2039–2057.
- Mahrt, L., and M. Ek, 1984: The influence of atmospheric stability on potential evaporation. *J. Climate Appl. Meteor.*, **23**, 222–234.
- , and H. L. Pan, 1984: A two-layer model of soil hydrology. *Bound.-Layer Meteor.*, **29**, 1–20.
- Mass, C. F., and Y. H. Kuo, 1998: Regional real-time numerical weather prediction: Current status and future potential. *Bull. Amer. Meteor. Soc.*, **79**, 253–263.
- McCumber, M. C., and R. A. Pielke, 1981: Simulation of the effects of surface fluxes of heat and moisture in a mesoscale numerical model soil layer. *J. Geophys. Res.*, **86**, 9929–9938.
- Miller, D. A., and R. A. White, 1998: A continuous United States multilayer soil characteristics data set for regional climate and hydrology modeling. *Earth Interactions*, **2**. [Available online at <http://EarthInteractions.org>.]
- Mintz, Y., 1984: The sensitivity of numerically simulated climates to land surface boundary conditions. *The Global Climate*, J. T. Houghton, Ed., Cambridge University Press, 79–105.
- Mitchell, K. E., 1994: GCIP initiatives in operational mesoscale modeling and data assimilation at NMC. Preprints, *Fifth Conf. on Global Change Studies*, Nashville, TN, Amer. Meteor. Soc., 192–198.
- Noilhan, J., and S. Planton, 1989: A simple parameterization of land surface processes for meteorological models. *Mon. Wea. Rev.*, **117**, 536–549.
- Oncley, S. P., and J. Dudhia, 1995: Evaluation of surface fluxes from MM5 using observations. *Mon. Wea. Rev.*, **123**, 3344–3357.
- Ookouchi, Y., M. Segal, R. C. Kessler, and R. Pielke, 1984: Evaluation of soil moisture effects of the generation and modification of mesoscale circulations. *Mon. Wea. Rev.*, **112**, 2281–2292.
- Paegle, J., K. C. Mo, and J. Noguez-Paegle, 1996: Dependence of simulated precipitation on surface evaporation during the 1993 United States summer floods. *Mon. Wea. Rev.*, **124**, 345–361.

- Pan, H.-L., and L. Mahrt, 1987: Interaction between soil hydrology and boundary-layer development. *Bound.-Layer Meteor.*, **38**, 185–202.
- Peters-Lidard, C. D., E. Blackburn, X. Liang, and E. F. Wood, 1998: The effect of soil thermal conductivity parameterization on surface energy fluxes and temperatures. *J. Atmos. Sci.*, **55**, 1209–1224.
- Pielke, R. A., T. J. Lee, J. H. Copeland, J. L. Eastman, C. L. Ziegler, and C. A. Finley, 1997: Use of USGS-provided data to improve weather and climate simulations. *Ecol. Appl.*, **7**, 3–21.
- Roads, J. O., S. C. Chen, M. Kamamitsu, and H. Juang, 1997: NCEP's water and energy budget analysis residuals. *J. Geophys. Res.*, in press.
- Rowntree, P. R., 1983: Sensitivity of GCM to land surface processes. *Proc. Workshop in Intercomparison of Large Scale Models for Extended Range Forecasts*, Reading, United Kingdom, ECMWF, 225–261.
- , and J. R. Bolton, 1983: Simulations of the atmospheric response to soil moisture anomalies over Europe. *Quart. J. Roy. Meteor. Soc.*, **109**, 501–526.
- Schaake, J. C., V. I. Koren, Q. Y. Duan, K. Mitchell, and F. Chen, 1996: A simple water balance model (SWB) for estimating runoff at different spatial and temporal scales. *J. Geophys. Res.*, **101**, 7461–7475.
- Sellers, P. J., 1987: Canopy reflectance, photosynthesis and transpiration. II. The role of biophysics in the linearity of their interdependence. *Remote Sens. Environ.*, **21**, 143–183.
- , Y. Mintz, Y. C. Sud, and A. Dalcher, 1986: A simple biosphere model (Sib) for use within general circulation models. *J. Atmos. Sci.*, **43**, 505–531.
- Shao, Y., and A. Henderson-Sellers, 1996: Modeling soil moisture: A project for for Intercomparison of Land Surface Parameterization Schemes Phase 2(b). *J. Geophys. Res.*, **101**, 7227–7250.
- Smirnova, T. G., J. M. Brown, and S. G. Benjamin, 1996: The soil component of the MAPS model: Description and performance in one- and three-dimensional applications. Preprints, *11th Conf. on Numerical Weather Prediction*, Norfolk, VA, Amer. Meteor. Soc., 259–261.
- Smith, C. B., M. N. Lakhtakia, W. J. Capehart, and T. N. Carlson, 1994: Initialization of soil-water content in regional-scale atmospheric prediction models. *Bull. Amer. Meteor. Soc.*, **75**, 585–592.
- Stewart, J. B., and S. B. Verma, 1992: Comparison of surface fluxes and conductances at two contrasting sites within the FIFE area. *J. Geophys. Res.*, **97**, 18 623–18 628.
- Troen, I., and L. Mahrt, 1986: A simple model of the atmospheric boundary layer: Sensitivity to surface evaporation. *Bound.-Layer Meteor.*, **37**, 129–148.
- Viterbo, P., and A. C. Beljaars, 1995: An improved land surface parameterization scheme in the ECMWF model and its validation. *J. Climate*, **8**, 2716–2748.
- , and P. Courtier, 1995: The importance of soil water for medium-range weather forecasting. Implication for data assimilation. *Proc. WMO Workshop on Imbalances of Slowly Varying Components of Predictable Atmospheric Motions*, Beijing, China, WMO, 121–130.
- Warner, T. T., D. F. Kibler, and R. L. Steinhart, 1991: Separate and coupled testing of meteorological and hydrological forecast models for the Susquehanna River Basin in Pennsylvania. *J. Appl. Meteor.*, **30**, 1521–1533.
- Wetzel, P., and J. T. Chang, 1987: Concerning the relationship between evapotranspiration and soil moisture. *J. Climate Appl. Meteor.*, **26**, 18–27.
- Wood, E. F., D. P. Lettenmaier, and V. G. Zartarian, 1992: A land-surface parameterization with subgrid for general circulation models. *J. Geophys. Res.*, **97**, 2717–2728.
- , and Coauthors, 1998: The project for Intercomparison of Land-surface Parameterization Schemes (PILPS). Phase 2(c) Red-Arkansas River Basin experiment: 1. Experiment description and summary intercomparisons. *Global Planet. Change*, **19**, 115–136.
- Xue, Y., P. J. Sellers, J. L. Kinter, and J. Shukla, 1991: A simplified biosphere model for global climate studies. *J. Climate*, **4**, 346–364.
- Yucel, I., W. J. Shuttleworth, J. Washburne, and F. Chen, 1998: Evaluating NCEP Eta Model-derived data against observations. *Mon. Wea. Rev.*, **126**, 1977–1991.
- Ziegler, C. L., W. J. Martin, R. A. Pielke, and R. Walko, 1995: A modeling study of the dryline. *J. Atmos. Sci.*, **52**, 263–285.
- Zilitinkevich, S., 1995: Non-local turbulent transport: Pollution dispersion aspects of coherent structure of convective flows. *Air Pollution Theory and Simulation, Air Pollution III*, H. Power, N. Moussiopoulos, and C. A. Brebbia, Eds., Vol. I, Computational Mechanics Publications, 53–60.